Research Article | Vol. 30, No. 18 / 29 Aug 2022 / Optics Express 32887
Optics EXPRESS

Reducing circuit complexity in optical quantum computation using 3D architectures

WEN-HAO ZHOU,[1,2] MADHAV KRISHNAN VIJAYAN,[3] XIAO-WEI WANG,[1,2] YONG-HENG LU,[1,2] JUN GAO,[1,2] ZHI-QIANG JIAO,[1,2] RUO-JING REN,[1,2] YI-JUN CHANG,[1,2] ZI-SONG SHEN,[1,2] PETER P. ROHDE,[3,4,6] AND XIAN-MIN JIN[1,2,5,*]

[1]*Center for Integrated Quantum Information Technologies (IQIT), School of Physics and Astronomy and State Key Laboratory of Advanced Optical Communication Systems and Networks, Shanghai Jiao Tong University, Shanghai 200240, China*
[2]*CAS Center for Excellence and Synergetic Innovation Center in Quantum Information and Quantum Physics, University of Science and Technology of China, Hefei, Anhui 230026, China*
[3]*Centre for Quantum Software & Information (UTS:QSI), University of Technology Sydney, Sydney NSW, Australia*
[4]*Hearne Institute for Theoretical Physics, Department of Physics & Astronomy, Louisiana State University, Baton Rouge, LA, USA*
[5]*TuringQ Co., Ltd., Shanghai 200240, China*
[6]*dr.rohde@gmail.com*
[*]*xianmin.jin@sjtu.edu.cn*

Abstract: Integrated photonic architectures based on optical waveguides are one of the leading candidates for the future realisation of large-scale quantum computation. One of the central challenges in realising this goal is simultaneously minimising loss whilst maximising interferometric visibility within waveguide circuits. One approach is to reduce circuit complexity and depth. A major constraint in most planar waveguide systems is that beamsplitter transformations between distant optical modes require numerous intermediate SWAP operations to couple them into nearest neighbour proximity, each of which introduces loss and scattering. Here, we propose a 3D architecture which can significantly mitigate this problem by geometrically bypassing trivial intermediate operations. We demonstrate the viability of this concept by considering a worst-case 2D scenario, where we interfere the two most distant optical modes in a planar structure. Using femtosecond laser direct-writing technology we experimentally construct a 2D architecture to implement Hong-Ou-Mandel interference between its most distant modes, and a 3D one with corresponding physical dimensions, demonstrating significant improvement in both fidelity and efficiency in the latter case. In addition to improving fidelity and efficiency of individual non-adjacent beamsplitter operations, this approach provides an avenue for reducing the optical depth of circuits comprising complex arrays of beamsplitter operations.

1. Introduction

Linear optics quantum computing [1] is one of the leading candidates for the realisation of scalable quantum computation. In this model, universal quantum circuits can be decomposed into series of unitary optical transformations, measurement and feedforward. Due to present-day technological limitations in which fast-feedforward is not yet viable, we are limited to passive linear optics. Despite ruling out universal quantum computation, passive linear optics is sufficient for implementing restricted computational models such as quantum walks [2,3] and boson-sampling [4–6], where the quantum advantage milestone has already been reached [5]. Such so-called noisy intermediate-scale quantum (NISQ) computers [7] have also been demonstrated in other architectures [8,9].

#464108 https://doi.org/10.1364/OE.464108
Journal © 2022 Received 22 May 2022; revised 6 Jul 2022; accepted 6 Jul 2022; published 24 Aug 2022

Optics EXPRESS

In the optical context, noise and loss in quantum gates limits the scalability of quantum circuits, thus optimising linear optics transformations to reduce loss and maximise interferometric visibility is a primary goal [10]. In the case of boson-sampling, this enables larger-scale demonstrations, whilst in the future context of fault-tolerant quantum computers [11], this reduces quantum error correction overheads [12,13], thereby improving scalability.

Integrated photonic waveguides are an attractive way to construct large-scale optical circuits owing to their inherent optical stability and miniaturization [14]. Additionally, significant progress has been made towards enabling dynamic reconfiguration of waveguide circuits [15]. The primary limitation is that waveguide architectures are largely limited to 2D planar constructions, by virtue of the fabrication technology. This planar constraint implies that implementing beamsplitter transformations between non-nearest neighbour optical modes requires intermediate trivial SWAP operations to bring them into proximity, each of which introduces inefficiency. In addition, in the 2D architecture, we need to finely control each beamsplitter ratio to obtain better interference results. The imperfection of any beamsplitter will affect the stability of the interference results.

In this paper, we demonstrate that 3D architectures are able to implement arbitrary beamsplitter operations between distant modes by geometrically bypassing intermediate modes, thereby significantly mitigating these limitations. Using femtosecond laser direct-writing technology, we construct two commonly used quantum gates: long-range SWAP gates; and long-range Hong-Ou-Mandel interference (i.e a 50:50 beamsplitter). We do so using both a 2D planar construction and a 3D construction, each with matching numbers of optical modes, physical dimensions and mode separations. We demonstrate that the 3D architecture, which bypasses intermediate trivial operations, reduces waveguide transmission loss and prevents the photons scattering into undesired modes, hence significantly improving fidelity and efficiency compared to the conventional 2D construction.

2. Experiment

Arbitrary quantum computations can be implemented optically using a combination of unitary linear optical transformations, measurement and fast-feedforward [1]. Here we focus on the former component. It was shown by Reck *et al.* [16] that any n-mode unitary optical transformation $\hat{U} \in \mathrm{SU}(n)$, implementing $\vec{a}^\dagger \rightarrow \hat{U} \cdot \vec{a}^\dagger$ on the associated vector of photonic creation operators $\vec{a}^\dagger$, can be decomposed into $O(n^2)$ beamsplitter and phase-shifter operations in a planar configuration.

A discrete-time beamsplitter operation, represented by an SU(2) mode transformation, can be realised using the continuous-time coupled oscillator Hamiltonian [17] of the form,

$$\hat{H} = \xi \hat{a}^\dagger \hat{b} + \xi^* \hat{a} \hat{b}^\dagger, \tag{1}$$

where $\hat{a}$ and $\hat{b}$ are the canonical mode operators and ξ is a complex interaction parameter characterising the interaction between two neighbouring modes. This Hamiltonian generates the unitary,

$$\hat{U} = e^{-i\hat{H}t}, \tag{2}$$

where $t = L/c$ is the interaction time, proportional to the interaction length L. The interaction length L determines the effective beamsplitter ratio, while wavelength-scale adjustments on the input and output modes control phase relationships, enabling arbitrary SU(2) beamsplitter operations to be implemented.

Currently, most photonic waveguide chips are manufactured on silicon wafers using well-established CMOS fabrication processes. This technology has the limitation of being confined to a 2D surface.

As shown in Fig. 1(a), if we want to interact modes k and m, which are not neighbouring modes, we require $(m - k - 1)$ completely transmissive beamsplitters (SWAP gates) to transport photons from mode k to neighbour mode m, then interact the two modes using an appropriate

Optics EXPRESS

beamsplitter, followed by another $(m-k-1)$ SWAP beamsplitters to transport back to mode k. The entire operation consumes $2(m-k)-1$ beamsplitters. Similarly, an arbitrary long-range beamsplitter operation can be implemented by adjusting the splitting ratio of the red beamsplitter.

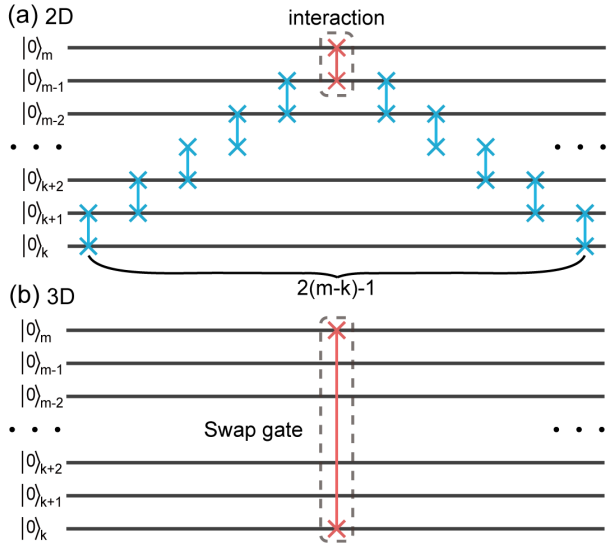

Fig. 1. Comparison of 2D and 3D architectures for the long-range SWAP gate. (a) For two distant modes k and m, $2(m-k)-1$ beamsplitters are required to implement the SWAP(k,m) gate. By adjusting the splitting ratio of the red beamsplitter, we can equivalently implement an arbitrary long-range beamsplitter. (b) Using the 3D architecture we can realize the same operation using only one single red beamsplitter.

It is intuitively clear that 3D routing enables these intermediate operations to be bypassed, allowing us to avoid the associated photons leakage and reduce experimental error. As shown in Fig. 1(b), if we are not constrained to two dimensions, we can route arbitrary modes directly without requiring trivial intermediate operations, allowing us to reduce the number of mode interactions required to implement the transformation, thereby improving the fidelity and efficiency of the circuit. In two dimensions, a SWAP operation between modes m and k, denoted $\hat{\pi}_{m,k}$, can be decomposed into a product of nearest-neighbour $\hat{\pi}_{i,i+1}$ SWAP operations,

$$\hat{\pi}_{m,k} = \hat{\pi}_{k,k+1}\hat{\pi}_{k+1,k+2}\ldots\hat{\pi}_{m-1,m}\hat{\pi}_{m-2,m-1}\ldots\hat{\pi}_{k,k+1}, \tag{3}$$

which contains $2(m-k)-1$ operations (see Supplement 1 for the derivation of this decomposition). In three dimensions, on the other hand, $\hat{\pi}_{m,k}$ can be implemented directly without further decomposition, requiring only 1 operation.

3. Results

Femtosecond laser direct-writing technology [18] provides an excellent platform for engineering 3D architectures, and has previously been used for demonstrating quantum walks [19–22], boson-sampling [23,24] and topological photonics [25,26].

To implement the long-range SWAP and beamsplitter operations, we first experimentally determine the effective beamsplitter ratio as a function of waveguide interaction length, as plotted in Fig. 2(a). These beamsplitters are fabricated in borosilicate glass (see Supplement 1 for details of the fabrication process). The spacing between input modes is 127μm, and the spacing of the coupling region is fixed at 8μm. In order to reduce loss associated with waveguide bending, arc formations with radius R = 30mm smoothly transition mode location.

Optics EXPRESS

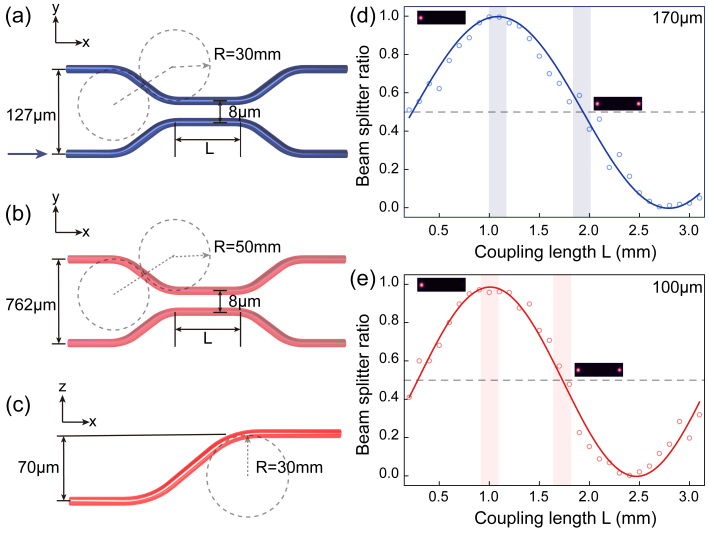

Fig. 2. Experimental parameter selection. (a) Beamsplitter implementation in the 2D architecture. (b) Beamsplitter implementation in the 3D architecture. Note the larger curvature radius, enabled by the simplified circuit structure. (c) Bending transformation along the z-axis (i.e chip depth) in the 3D architecture. (d) Beamsplitter ratio as a function of coupling length L at 170μm depth for the 2D case. (e) Beamsplitter ratio as a function of coupling lengths L at 100μm depth for the 3D case.

We inject coherent light (via a $\lambda = 780$nm semiconductor laser) into the beamsplitter as per Fig. 2(a), capturing the output intensity distribution with a CCD camera. We extract the intensities I_1 and I_2 of the two output modes, from which the beamsplitter ratio is determined as $r = I_2/I_1$.

By sweeping through different coupling lengths L at two different depths along the chip's z-axis (170μm and 100μm), we obtain two beamsplitter ratio curves, shown in Figs. 2(d,e). From this we establish the approximate regimes for the 100:0 and 50:50 beamsplitter ratios. For the two distant modes in the 3D architecture, we have the topological liberty to increase the curvature radius to $R = 50$mm, enabling a reduction in associated loss, as per Fig. 2(b). Figure 2(c) illustrates the bending transformation between 170μm and 100μm under the upper surface of the chip.

In Fig. 3(a), we show the waveguide structure of the long-range SWAP gate in both the 2D and 3D architectures. Considering the loss and chip length (10cm), we set the waveguide number to $N = 7$. Waveguide coloring denotes distinct optical paths. In the 2D architecture all waveguides are at the same depth of 170μm, and in the 3D architectures we transform the two waveguides on the outermost side to 100μm depths. Multiple samples were fabricated to obtain the best swapping effect by finely scanning parameters within the windows described in Fig. 2(d,e).

We measure the output intensity distributions of modes 1, 4 and 7 respectively. As shown in Fig. 3(a), in the 2D architecture a small amount of light intensity scatters into undesired output modes, constituting leakage errors. We define the fidelity [27],

$$F = \sum_{i=1}^{N} \sqrt{e_i t_i}, \tag{4}$$

Optics EXPRESS

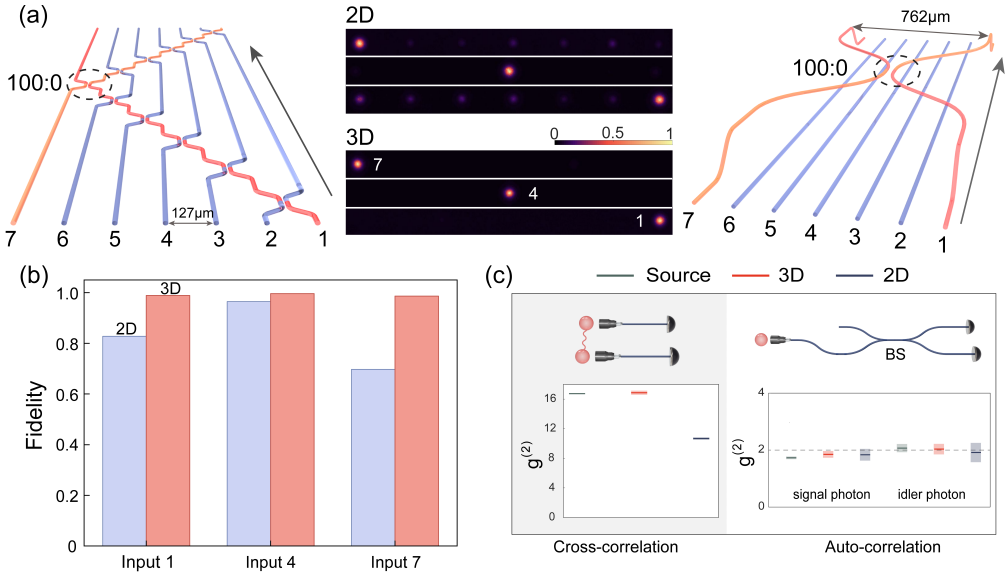

Fig. 3. Long-range SWAP gate. (a) Optical paths involved in the SWAP gate for the 2D (left) and 3D (right) architectures. Red and orange represent paths involved in the interaction, and blue represents paths not involved. The central figure shows the output intensity distributions (columns represent output mode-number) when single photons enter input modes 1, 4 and 7 respectively (represented by the three different rows), taken with a CCD camera. (b) Gate fidelity, comparing the 2D and 3D architectures, demonstrating improved fidelity in the 3D case. (c) Cross- and auto-correlation measurement results. The cross-correlation in the 2D architecture demonstrates a clear decline compared to the 3D architecture. The auto-correlation demonstrates no significant change between the 2D and 3D cases. The auto-correlation and cross-correlation plots share the same horizontal axes.

To quantify the operation of the SWAP operation, where e_i is the experimental probability distribution and t_i the theoretical probability distribution for the ith waveguide, extracted from Fig. 3(a).

Our results are shown in Fig. 3(b). Choosing three different paths, the fidelity of the 3D architecture is always above 98%. In contrast, if we choose inputs 1 or 7 in the 2D architecture, six intermediate 100:0 beamsplitters are required, significantly reducing fidelity. Choosing input 4, this only requires two 100:0 beamsplitters and the fidelity improves, remaining above 95%, still worse than the respective 3D architecture. We can define the fidelity of a single beamsplitter as η and estimate the fidelity of a series of n beamsplitters scales as η^n. The fidelity of the long-range SWAP gate in the 2D architecture therefore decreases exponentially with the number of intermediate beamsplitters (equivalently their separation), which the 3D architecture mitigates.

The auto-correlation $g^{(2)}_{s-s}$, $g^{(2)}_{i-i}$ and cross-correlation functions $g^{(2)}_{s-i}$ [28] provide confirmation of single-photon states and two-photon correlations. The correlation function $g^{(2)}_{xy}$ is defined by,

$$g^{(2)}_{xy} = \frac{N_{xy}N_p}{N_x N_y}, \tag{5}$$

where N_{xy} represents coincidence detection counts, N_x single-mode detection counts, and N_p the laser repetition rate.

To measure the cross-correlation, we inject a pair of $\lambda = 780$nm correlated photons generated by spontaneous parametric down conversion (SPDC) [29] (see Supplement 1 for details) into input

Optics EXPRESS

modes 1 and 7, detecting coincidence counts between the respective output modes. As shown in Fig. 3(c), the $g^{(2)}_{s-i} = 16.86 \pm 0.27$ of the 3D architecture is very close to the $g^{(2)}_{source} = 16.74 \pm 0.06$, well above the classical bound of $g^{(2)}_{s-i} = 2$. The $g^{(2)}_{s-i}$ of the 2D architecture decreases to 10.67 ± 0.19, owing to scattering into undesired outputs.

To measure the auto-correlation, we inject the SPDC signal and idler photons into input 1 separately, measuring coincidence counts following a balanced fiber beamsplitter, as shown in Fig. 3(c). The auto-correlation should ideally be 2 for single-photon behavior. Compared with the quantum source, the $g^{(2)}_{s-s}$ and $g^{(2)}_{i-i}$ for both the 2D and 3D architectures exhibit no significant difference.

Next we implement Hong-Ou-Mandel interference [30] between the two most spatially distant modes in a circuit. In Fig. 4(a), we illustrate the respective waveguide structures where red denotes the expected optical paths. In the 2D architecture, these paths are subject to additional bending transformations compared to the 3D case, resulting in increased loss and scattering. In the 3D architecture these intermediate modes are bypassed, enabling direct interference between the desired modes with improved visibility.

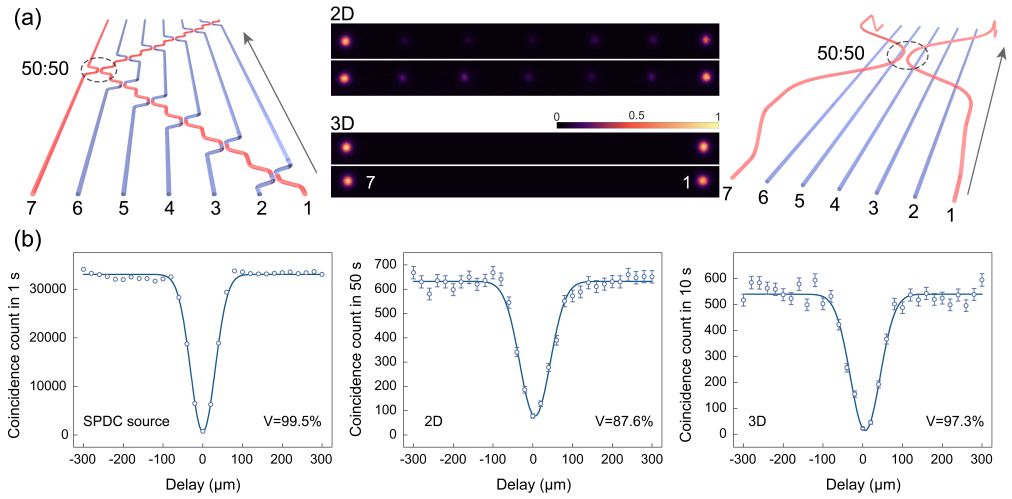

Fig. 4. Hong-Ou-Mandel interference via a long-range beamsplitter. (a) Optical paths using the same convention as per Fig. 3(a), however now we replace the 100:0 beamsplitter (i.e SWAP gate) with a 50:50 beamsplitter and employ a two-photon input state, with one photon at each of the input modes 1 and 7. The central CCD plots show the input and output intensities. In the 2D case the output intensity distribution demonstrates leakage into undesired modes (2-6), whereas in the 3D case leakage is negligible. (b) Hong-Ou-Mandel fringes and their associated HOM-visibility for the SPDC source alone (left), the 2D architecture (middle), and the 3D architecture (right). The 3D architecture demonstrates substantially higher HOM-visibility (97.3%) than the 2D architecture (87.6%), and roughly a five-fold improvement in count-rates, indicative of reduced loss.

We characterize the performance of both architectures by measuring their Hong-Ou-Mandel visibility. We inject photon pairs into input modes 1 and 7, measuring coincidence rates against introduced relative temporal delays, from which we calculate their HOM visibilities, shown in Fig. 4(b). Comparing these against the HOM visibility obtained directly from the SPDC source (i.e without the waveguide chip), the 3D architecture retains high visibility, whereas for the 2D architecture the visibility is significantly reduced and total count rates are reduced by a factor of ~ 5 due to lower chip efficiency. For larger circuits where many modes repeatedly interfere with each other in both 2D and 3D structures, different bending transformations will introduce

Optics EXPRESS

additional phases. By changing the deformation coefficient [31] such as curvature radius R or adding the thermal regulation [32], we can quantitatively control the phase-shift and compensate for the accumulated phases.

4. Conclusions and discussions

In summary, we present a proof-of-principle construction of a 3D architecture demonstrating significant improvement in efficiency and interference visibility compared to an equivalent 2D construction. Our proof-of-principle demonstration is based on considering the worst-case scenario of interfering the two most distant optical modes in a waveguide chip. By eliminating redundant operations, 3D architectures enable simplification of optical circuits and the mitigation of errors associated with redundant operations. The 3D structure reduces unnecessary bending transformations in the circuit, so the transmission loss is smaller. On the other hand, the 3D structure expand the experimental dimension. We can make any two waveguides perform a gate operation at different depths and then return to the same depth, which provides the possibility of parallel operation. Since there is no intermediate coupling process, the waveguides do not affect each other, so the 3D structure can achieve smaller scattering losses and obtain higher fidelity.

The limitation of our model is that we consider fixed circuit structures, which is only applicable for static circuits with a priori knowledge of the circuit structure. More advanced 3D architectures will need to incorporate tunable beamsplitters to enable both reconfigurable circuits and the fast-feedforward operations necessary for universal optical quantum computation.

Given that large-scale optical circuits can always be decomposed into sequences of two-mode transformations, it is expected that more complex optical circuits comprising multiple pairwise transformations will exhibit greater improvement, given that total efficiency and fidelity scale exponentially with the number of constituent operations. Therefore, the 3D architecture has the potential application in quantum network [33], multistage entanglement swapping [34] and large-scale quantum circuits.

Funding. National Key Research & Development Program of China (2019YFA0706302, 2019YFA0308700, 2017YFA0303700); National Natural Science Foundation of China (11904229, 61734005, 11761141014, 11690033); Science and Technology Commission of Shanghai Municipality (STCSM) (2019SHZDZX01, 20JC1416300); Shanghai Municipal Education Commission (SMEC) (2017-01-07-00-02-E00049); China Postdoctoral Science Foundation (2020M671091); ARC Future Fellowship (project FT160100397) conducted by the ARC Centre of Excellence for Engineered Quantum Systems (project CE170100009).

Acknowledgments. X.-M.J. acknowledges additional support from a Shanghai talent program and support from Zhiyuan Innovative Research Center of Shanghai Jiao Tong University.

Disclosures. The authors declare no conflicts of interest.

Data availability. Data underlying the results presented in this paper are not publicly available at this time but may be obtained from the authors upon reasonable request.

Supplemental document. See Supplement 1 for supporting content.

References

1. E. Knill, R. Laflamme, and G. J. Milburn, "A scheme for efficient quantum computation with linear optics," Nature **409**(6816), 46–52 (2001).
2. A. M. Childs, "Universal computation by quantum walk," Phys. Rev. Lett. **102**(18), 180501 (2009).
3. A. Schreiber, A. Gábris, P. P. Rohde, K. Laiho, M. Štefanák, V. Potocek, C. Hamilton, I. Jex, and C. Silberhorn, "A 2d quantum walk simulation of two-particle dynamics," Science **336**(6077), 55–58 (2012).
4. S. Aaronson and A. Arkhipov, "The computational complexity of linear optics," in *Proc. 43rd Ann. Symp. on Theory of Computing*, (2011), p. 333.
5. H.-S. Zhong, H. Wang, and Y.-H. Deng, *et al.*, "Quantum computational advantage using photons," Science **370**(6523), 1460–1463 (2020).
6. H.-S. Zhong, Y.-H. Deng, and J. Qin, *et al.*, "Phase-programmable gaussian boson sampling using stimulated squeezed light," Phys. Rev. Lett. **127**(18), 180502 (2021).
7. J. Preskill, "Quantum computing in the nisq era and beyond," Quantum **2**, 79 (2018).

Optics EXPRESS

8. F. Arute, K. Arya, and R. Babbush, *et al.*, "Quantum supremacy using a programmable superconducting processor," Nature **574**(7779), 505–510 (2019).
9. Y. Wu, W.-S. Bao, and S. Cao, *et al.*, "Strong quantum computational advantage using a superconducting quantum processor," Phys. Rev. Lett. **127**(18), 180501 (2021).
10. B. Nash, V. Gheorghiu, and M. Mosca, "Quantum circuit optimizations for nisq architectures," Quantum Sci. Technol. **5**(2), 025010 (2020).
11. M. A. Nielsen and C. M. Dawson, "Fault-tolerant quantum computation with cluster states," Phys. Rev. A **71**(4), 042323 (2005).
12. J. Chiaverini, D. Leibfried, T. Schaetz, M. D. Barrett, R. Blakestad, J. Britton, W. M. Itano, J. D. Jost, E. Knill, C. Langer, R. Ozeri, and D. J. Wineland, "Realization of quantum error correction," Nature **432**(7017), 602–605 (2004).
13. B. M. Terhal, "Quantum error correction for quantum memories," Rev. Mod. Phys. **87**(2), 307–346 (2015).
14. A. Peruzzo, M. Lobino, J. C. F. Matthews, N. Matsuda, A. Politi, K. Poulios, X.-Q. Zhou, Y. Lahini, N. Ismail, K. Wörhoff, Y. Bromberg, Y. Silberberg, M. G. Thompson, and J. L. OBrien, "Quantum walks of correlated photons," Science **329**(5998), 1500–1503 (2010).
15. J. Carolan, C. Harrold, C. Sparrow, E. Martín-López, N. J. Russell, J. W. Silverstone, P. J. Shadbolt, N. Matsuda, M. Oguma, M. Itoh, G. D. Marshall, M. G. Thompson, J. C. F. Matthews, T. Hashimoto, J. L. O'Brien, and A. Laing, "Universal linear optics," Science **349**(6249), 711–716 (2015).
16. M. Reck, A. Zeilinger, H. J. Bernstein, and P. Bertani, "Experimental realization of any discrete unitary operator," Phys. Rev. Lett. **73**(1), 58–61 (1994).
17. C. Gerry and P. Knight, *Introductory Quantum Optics* (Cambridge University Press, 2005).
18. K. M. Davis, K. Miura, N. Sugimoto, and K. Hirao, "Writing waveguides in glass with a femtosecond laser," Opt. Lett. **21**(21), 1729 (1996).
19. Z.-Q. Jiao, J. Gao, W.-H. Zhou, X.-W. Wang, R.-J. Ren, X.-Y. Xu, L.-F. Qiao, Y. Wang, and X.-M. Jin, "Two-dimensional quantum walks of correlated photons," Optica **8**(9), 1129 (2021).
20. K. Poulios, R. Keil, D. Fry, J. D. Meinecke, J. C. Matthews, A. Politi, M. Lobino, M. Gräfe, M. Heinrich, S. Nolte, A. Szameit, and J. L. O'Brien, "Quantum walks of correlated photon pairs in two-dimensional waveguide arrays," Phys. Rev. Lett. **112**(14), 143604 (2014).
21. H. Tang, X.-F. Lin, Z. Feng, J.-Y. Chen, J. Gao, K. Sun, C.-Y. Wang, P.-C. Lai, X.-Y. Xu, Y. Wang, L.-F. Qiao, A.-L. Yang, and X.-M. Jin, "Experimental two-dimensional quantum walk on a photonic chip," Sci. Adv. **4**(5), eaat3174 (2018).
22. M. Ehrhardt, R. Keil, L. J. Maczewsky, C. Dittel, M. Heinrich, and A. Szameit, "Exploring complex graphs using three-dimensional quantum walks of correlated photons," Sci. Adv. **7**(9), eabc5266 (2021).
23. J. Gao, Z.-Q. Jiao, R.-J. Ren, X.-W. Wang, X.-Y. Xu, W.-H. Zhou, L.-F. Qiao, and X.-M. Jin, "Experimental collision-free dominant boson sampling," arXiv preprint arXiv:1910.11320 (2019).
24. W.-H. Zhou, J. Gao, Z.-Q. Jiao, X.-W. Wang, R.-J. Ren, X.-L. Pang, L.-F. Qiao, C.-N. Zhang, T.-H. Yang, and X.-M. Jin, "Timestamp boson sampling," arXiv preprint arXiv:2009.03327 (2020).
25. M. C. Rechtsman, J. M. Zeuner, Y. Plotnik, Y. Lumer, D. Podolsky, F. Dreisow, S. Nolte, M. Segev, and A. Szameit, "Photonic floquet topological insulators," Nature **496**(7444), 196–200 (2013).
26. Y. Wang, Y.-H. Lu, F. Mei, J. Gao, Z.-M. Li, H. Tang, S.-L. Zhu, S. Jia, and X.-M. Jin, "Direct observation of topology from single-photon dynamics," Phys. Rev. Lett. **122**(19), 193903 (2019).
27. M. A. Nielsen and I. Chuang, "Quantum computation and quantum information," (2002).
28. M. Fox, *Quantum optics: an introduction*, vol. 15 (OUP Oxford, 2006).
29. M. H. Rubin, D. N. Klyshko, Y. Shih, and A. Sergienko, "Theory of two-photon entanglement in type-ii optical parametric down-conversion," Phys. Rev. A **50**(6), 5122–5133 (1994).
30. C.-K. Hong, Z.-Y. Ou, and L. Mandel, "Measurement of subpicosecond time intervals between two photons by interference," Phys. Rev. Lett. **59**(18), 2044–2046 (1987).
31. A. Crespi, R. Osellame, R. Ramponi, D. J. Brod, E. F. Galvao, N. Spagnolo, C. Vitelli, E. Maiorino, P. Mataloni, and F. Sciarrino, "Integrated multimode interferometers with arbitrary designs for photonic boson sampling," Nat. Photonics **7**(7), 545–549 (2013).
32. F. Flamini, L. Magrini, and A. S. Rab, *et al.*, "Thermally reconfigurable quantum photonic circuits at telecom wavelength by femtosecond laser micromachining," Light: Sci. Appl. **4**(11), e354 (2015).
33. J. I. Cirac, P. Zoller, H. J. Kimble, and H. Mabuchi, "Quantum state transfer and entanglement distribution among distant nodes in a quantum network," Phys. Rev. Lett. **78**(16), 3221–3224 (1997).
34. A. M. Goebel, C. Wagenknecht, Q. Zhang, Y.-A. Chen, K. Chen, J. Schmiedmayer, and J.-W. Pan, "Multistage entanglement swapping," Phys. Rev. Lett. **101**(8), 080403 (2008).